Available online at www.sciencedirect.com
ScienceDirect
Journal of Computational Physics 218 (2006) 635–653
JOURNAL OF COMPUTATIONAL PHYSICS
www.elsevier.com/locate/jcp

A numerical algorithm for kinetic modelling of evaporation processes

I.N. Shishkova [a], S.S. Sazhin [b,*]

[a] *Low Temperature Department, Centre of High Technologies, Moscow Power Engineering Institute, Krasnokazarmennaya, 14, Moscow 111250, Russia*
[b] *School of Engineering, Faculty of Science and Engineering, University of Brighton, Cockcroft Building, Lewes Road, Brighton, East Sussex BN2 4GJ, United Kingdom*

Received 11 August 2005; received in revised form 21 February 2006; accepted 27 February 2006
Available online 2 May 2006

Abstract

A numerical algorithm for kinetic modelling of droplet evaporation processes is suggested. This algorithm is focused on the direct numerical solution of the Boltzmann equations for two gas components: vapour and air. The physical and velocity spaces are discretised, and the Boltzmann equations are presented in discretised forms. The solution of these discretised equations is performed in two steps. Firstly, molecular displacements are calculated ignoring the effects of collisions. Secondly, the collisional relaxation is calculated under the assumption of spatial homogeneity. The conventional approach to calculating collisional integrals is replaced by the integration based on random cubature formulae. The distribution of molecular velocities after collisions is found based on the assumption that the total impulse and energy of colliding molecules are conserved. The directions of molecular impulses after the collisions are random, but the values of these impulses belong to an a priori chosen set. A new method of finding the matching condition for vapour mass fluxes at the outer boundary of the Knudsen layer of evaporating droplets and at the inner boundary of the hydrodynamic region is suggested. The numerical algorithm is applied to the analysis of three problems: the relaxation of an initially non-equilibrium distribution function towards the Maxwellian one, the analysis of the mixture of vapour and inert gas confined between two infinite plates and the evaporation of a diesel fuel droplet into a high pressure air. The solution of the second problem showed an agreement between the results predicted by the widely used Bird's algorithm and the algorithm described in this paper. In the third problem the difference of masses and radii of vapour and air molecules is taken into account. The kinetic effects predicted by the numerical algorithm turned out to be noticeable if the contribution of air in the Knudsen layer is taken into account.

Keywords: Kinetic modelling; Evaporation; Binary mixture; Boltzmann equations; Direct numerical solution

* Corresponding author. Tel.: +44 1273 642677; fax: +44 1273 642301.
E-mail address: S.Sazhin@brighton.ac.uk (S.S. Sazhin).

0021-9991/$ - see front matter © 2006 Elsevier Inc. All rights reserved.
doi:10.1016/j.jcp.2006.02.019

1. Introduction

The importance of accurate kinetic modelling of the gas (non-ionised or ionised) dynamics in physics, engineering and environmental applications is widely recognised [1–7]. This analysis is simplified in the case when the characteristic scales of the problem are much larger or much smaller than the mean free path of molecules. In the first case the kinetic Boltzmann equation is reduced to well known hydrodynamic equations, while in the second case the analysis of this equation is greatly simplified due to the fact that collision processes can be ignored. Notwithstanding these two limiting cases, the kinetic analysis of gas dynamics needs to be based on the solution of the Boltzmann equation, taking into account the collision processes. Note that the Boltzmann equation itself is an approximation of the more general chain of Bogolubov–Born–Green–Kirkwood–Yvon (BBGKY) chain of equations [5].

A number of approximate methods of the solution of the Boltzmann equation have been suggested. One of these methods is based on the replacement of this equation by the system of equations for the moments of the distribution function [2]. Although this method is important from the point of view of theoretical developments, its practical applications to non-stationary and multi-dimensional problems are limited. An alternative approximate method is widely known as the method of the model kinetic equations. In this method, the actual collision integral is not calculated but modelled. One of the most widely used variations of this method was suggested in [8] and is known as Bhatnagar–Gross–Krook (BGK) method (cf. [9,10]). More advanced versions of the method of the model kinetic equations were suggested by Shakhov and described in [11]. These methods are computationally economical but their accuracy becomes poor when the distribution of gas molecules (ions/electrons) deviates considerably from the equilibrium distribution. A more detailed analysis of these approximate methods and the results of their applications are reviewed in a number of monographs and papers including [12–14]. Although these solutions have proven to be useful in qualitative analysis of phenomena and understanding of the underlying physics, their limitations for the quantitative analysis are well known.

It seems that the only way to perform the quantitative analysis of gas dynamics in the general case can be based on direct numerical methods. For non-ionised gases such methods were developed by Bird [15,16] and Aristov and Tcheremissine [17]. Bird based his approach on direct statistical analyses of the dynamics of individual atoms while Aristov and Tcheremissine developed a new method of the direct numerical solution of the Boltzmann equation. These methods were further developed and applied to the analysis of gas dynamics, including evaporation and condensation problems in numerous papers including [17–29]. Attempts to apply these methods to binary mixtures were reported in [23–28]. Numerical difficulties in the analysis of these mixtures, however, led to imposing a number of restrictions on the properties of molecules. Molecules considered in [23,25,26] were assumed to be mechanically identical. In [24,27] the difference in the masses of molecules was taken into account but their diameters were assumed to be the same. These assumptions can hardly be justified in many practical engineering applications, where molecules in binary mixtures have very different diameters (cf. the problem of evaporation of heavy hydrocarbons into air). No attempts to solve the Boltzmann equations for a mixture of more than 2 gases have been reported to the best of our knowledge.

The main aim of this paper is to present a numerical algorithm for the solution of the Boltzmann equations which was originally suggested in [17] and applied to the solution of Boltzmann equations for 2 gases in [28,30]. Some new features of this algorithm, including those referring to the calculation of the collision integral for binary mixtures, will be discussed. This algorithm is applied to simulate the dynamics of binary mixtures without making an assumption that masses or sizes of all molecules are identical. The physical background and mathematical formulation of the problem are presented and discussed in Section 2. The numerical algorithm for the solution of the basic equations is described in Section 3. In Section 4 the properties of the Knudsen layer around evaporating droplets and the matching of the kinetic solution in this layer with the hydrodynamic solution in the ambient gas are investigated. The results of testing and application of the model and numerical algorithm to several engineering problems are presented and discussed in Section 5. The main results of the paper are summarised in Section 6.

2. Basic equations and approximations

For the analysis of molecular dynamics we assume that gas molecules are colliding elastic spheres characterised by the distribution function $f(\mathbf{r},t,\mathbf{v}) : f(\mathbf{r},t,\mathbf{v})\mathrm{d}\mathbf{r}\,\mathrm{d}\mathbf{v}$ is the expected number of molecules located between $\mathbf{r}$ and $\mathbf{r}+\mathrm{d}\mathbf{r}$ in the physical space and between $\mathbf{v}$ and $\mathbf{v}+\mathrm{d}\mathbf{v}$ in the velocity space at the moment of time t. The assumption about elastic spheres will be relaxed when the details of the collision processes are studied. We assume that two types of molecules are present in the system characterised by two distribution functions $f_\mathrm{a}(\mathbf{r},t,\mathbf{v})$ and $f_\mathrm{b}(\mathbf{r},t,\mathbf{v})$. Each of these functions depends on 7 variables (3 components of $\mathbf{r}$ (x,y,z), 3 components of $\mathbf{v}$ (v_x,v_y,v_z) and t) in the general case.

The evolution of f_a and f_b is controlled by the corresponding Boltzmann equations:

$$\left.\begin{aligned}\frac{\partial f_\mathrm{a}}{\partial t}+\mathbf{v}_\mathrm{a}\frac{\partial f_\mathrm{a}}{\partial \mathbf{r}} &= J_\mathrm{aa}+J_\mathrm{ab}\\ \frac{\partial f_\mathrm{b}}{\partial t}+\mathbf{v}_\mathrm{b}\frac{\partial f_\mathrm{b}}{\partial \mathbf{r}} &= J_\mathrm{ba}+J_\mathrm{bb}\end{aligned}\right\}, \tag{1}$$

where $J_{\alpha\beta}$ ($\alpha=a,b$; $\beta=a,b$) are collision integrals defined as

$$J_{\alpha\beta}=\frac{\sigma_{\alpha\beta}^2}{2}\int_{-\infty}^{+\infty}\mathrm{d}\mathbf{v_1}\int_0^{\pi}\sin\theta\,\mathrm{d}\theta\int_0^{2\pi}\mathrm{d}\phi\left(f'_\alpha f'_{\beta1}-f_\alpha f_{\beta1}\right)|\mathbf{v}_\alpha-\mathbf{v}_{\beta1}|, \tag{2}$$

$\sigma_{\alpha\beta}=(\sigma_\alpha+\sigma_\beta)/2$, σ_α and σ_β are the corresponding diameters of molecules, θ and ϕ are angular coordinates of molecules β relative to molecules α, superscript $'$ indicates the velocities and the distribution functions after collisions, subscript $_1$ indicates that the function f_α is modified under the influence of collisions with molecules of the type $_\beta$. The first integral in the right hand side of (2) is calculated in the three dimensional velocity space. When deriving (1), it was assumed that body forces acting on molecules are negligible.

In order to calculate the integrals in (2), one needs to know the distribution functions f'_α and $f'_{\beta1}$ after collisions. To do this, it is necessary to establish the relation between $\mathbf{v}_\alpha$, $\mathbf{v}_{\beta1}$ on one side and $\mathbf{v}'_\alpha$, $\mathbf{v}'_{\beta1}$ on the other side. The analysis of the collision processes is based on the assumption that collisions are elastic. In this case the laws of conservation of impulse and energy lead to the following system of equations for $\mathbf{v}'_\alpha$ and $\mathbf{v}'_{\beta1}$ [31]:

$$\left.\begin{aligned}\mathbf{v}'_\alpha &= \frac{m_\beta}{m_\alpha+m_\beta}\left|\mathbf{v}'_\alpha-\mathbf{v}'_{\beta1}\right|\mathbf{n}_0+\frac{m_\alpha\mathbf{v}_\alpha+m_\beta\mathbf{v}_{\beta1}}{m_\alpha+m_\beta}\\ \mathbf{v}'_{\beta1} &= -\frac{m_\alpha}{m_\alpha+m_\beta}\left|\mathbf{v}'_\alpha-\mathbf{v}'_{\beta1}\right|\mathbf{n}_0+\frac{m_\alpha\mathbf{v}_\alpha+m_\beta\mathbf{v}_{\beta1}}{m_\alpha+m_\beta}\end{aligned}\right\}, \tag{3}$$

where m_α and m_β are the masses of molecules, $\mathbf{n}_0$ is the unit vector in the direction of molecular velocity after the collision in the frame of reference linked with the centre of inertia of colliding molecules.

In order to specify the value of $\mathbf{n}_0$, we would need to model the collision process itself for given relative velocities of molecules and their shapes. This is expected to be a very complicated task and the approximation of molecules by elastic spheres is likely to become questionable. Slight changes of the shape of molecules and their relative velocities before the collision process are likely to lead to substantial changes of the directions of their velocities after collisions. In this case, it seems logical to assume that $\mathbf{n}_0$ is a random parameter. The details of the numerical implementation of this model are discussed in Section 3. Equations for two molecular species are solved subject to boundary and initial conditions, determined for a specific problem (evaporation, condensation, heat transfer etc.) (see Section 4).

Once the values of the distribution function in various points in the physical space and at a certain moment of time are found, we can calculate the moments of these function. These are the examples of these moments which are most important from the point of view of applications:

$$n_\alpha=\int f_\alpha\,\mathrm{d}\mathbf{v}$$

(number density of gas α);

$$\rho_\alpha=m_\alpha\int f_\alpha\,\mathrm{d}\mathbf{v}$$

(mass density of gas α, m_α is the mass of individual molecules);

$$u_{i\alpha} = \frac{1}{n_\alpha}\int v_i f_\alpha \,\mathrm{d}\mathbf{v}$$

(*i*th component of the average velocity of molecules in gas α);

$$j_{i\alpha} = m_\alpha \int v_i f_\alpha \,\mathrm{d}\mathbf{v}$$

(mass flux of gas α in the direction *i*);

$$P_{ij\alpha} = \frac{m_\alpha}{2}\int (v_j - u_j)(v_i - u_i) f_\alpha \mathrm{d}\mathbf{v}$$

(components of the stress tensor of gas α);

$$T_\alpha = \frac{m_\alpha}{3 n_\alpha k_\mathrm{B}}\int (\mathbf{v} - \mathbf{u})^2 f_\alpha \mathrm{d}\mathbf{v}$$

(temperature of gas α; k_B is the Boltzmann constant);

$$q_{i\alpha} = \frac{m_\alpha}{2}\int (\mathbf{v} - \mathbf{u})^2 (v_i - u_i) f_\alpha \mathrm{d}\mathbf{v}$$

(heat flux of gas α in the direction *i*). Indices *i* and *j* refer to *x*, *y* and *z*.

The importance of these moments is based on the fact that they represent physically measurable parameters. Some of them (mass density and mass flux) will be extensively used in the following analysis.

3. Numerical algorithm

Our numerical algorithm is based on the method of direct numerical solution of the Boltzmann equation, described in [17,30]. It includes the following steps. Physical and velocity spaces are discretised along with time. Time and physical space are discretised as in conventional structured computational fluid dynamics (CFD) codes. The discretisation of the velocity space is performed similarly to the physical space via replacing continuous values of $\mathbf{v}$ by a discrete set $\{\mathbf{v}^k\}^M$, where *k* indicates the position of a velocity cell, *M* is the total number of cells. The boundaries of the velocity domain in v_x,v_y,v_z directions are chosen in such a way that the contribution of molecules with velocities outside this range can be ignored. In most practical implementations of the algorithm, the difference between minimal and maximal values of the velocities was taken equal to 5 or 6 average thermal speeds $\sqrt{2R_\alpha T_\alpha}$. Due to the difference in R_α for different gas components, the ranges of velocities for these components are also different.

For each value of $\mathbf{v}_\alpha^k$, the corresponding value of f_α^k is specified. This allows us to present Eq. (1) for each gas component in a discretised form:

$$\left\{\begin{array}{l} \frac{\Delta f_\alpha^1}{\Delta t} + \mathbf{v}_\alpha^1 \frac{\Delta f_\alpha^1}{\Delta \mathbf{r}} = J_{\alpha\alpha}^1 + J_{\alpha\beta}^1 \\ \ldots\ldots\ldots\ldots\ldots\ldots\ldots \\ \frac{\Delta f_\alpha^k}{\Delta t} + \mathbf{v}_\alpha^k \frac{\Delta f_\alpha^k}{\Delta \mathbf{r}} = J_{\alpha\alpha}^k + J_{\alpha\beta}^k \\ \ldots\ldots\ldots\ldots\ldots\ldots\ldots \\ \frac{\Delta f_\alpha^M}{\Delta t} + \mathbf{v}_\alpha^M \frac{\Delta f_\alpha^M}{\Delta \mathbf{r}} = J_{\alpha\alpha}^M + J_{\alpha\beta}^M \end{array}\right\}^M . \tag{4}$$

The boundary and initial conditions for the distribution functions are taken into account.

After calculation of $J_{\alpha\beta}^k$ for each cell $\mathbf{v}_\alpha^k$, the non-linear system of integral-differential equation (1) reduces to the linear system of algebraic Eq. (4), presented for both gas components. Following [17], the numerical solution of System (4) is performed in two steps. Firstly, molecular displacements are calculated ignoring the effect of collisions ($J_{\alpha\alpha}^k = J_{\alpha\beta}^k = 0$). Secondly, the collisional relaxation is calculated under the assumption of spatial homogeneity.

The numerical solution of Eq. (4) at the first step is performed following the explicit approach. The validity of the Courant condition:

$$\Delta t \max(|v_x|, |v_y|, |v_z|) < \min(\Delta x, \Delta y, \Delta z) \tag{5}$$

is assumed. Condition (5) guarantees that even the fastest molecules cannot cross more than one cell boundary in any of the directions x, y or z. Although explicit schemes are criticised for the lack of stability and relatively low accuracy in CFD applications, they proved to be acceptable for the solution of the Boltzmann equation. They are conservative, easy to implement and their physical meaning is rather clear. Due to the absence of collisions, the dynamics of each gas component is not influenced by another component.

At the next step, the displacement of molecules stops and they start colliding. Again using the explicit approach, each equation in System (4) can be written as:

$$\frac{f_\alpha^{k,n} - \tilde{f}_\alpha^{k,n-1}}{\Delta t} = J_{\alpha\alpha}^{k,n-1} + J_{\alpha\beta}^{k,n-1}, \tag{6}$$

where ~ indicates the value of the distribution function calculated at the first step, additional superscripts $^{n-1}$ and ^{n} indicate consecutive time steps. Eq. (6) are to be solved in each cell in the physical space.

For numerical solution of Eq. (1), $J_{\alpha\beta}$ were rewritten as:

$$J_{\alpha\beta} = -\nu_{\alpha\beta} f_\alpha + N_{\alpha\beta}, \tag{7}$$

where

$$\left.\begin{aligned} \nu_{\alpha\beta} &= \tfrac{\sigma_{\alpha\beta}^2}{2} \int_{-\infty}^{+\infty} \mathrm{d}\mathbf{v_1} \int_0^\pi \sin\theta \,\mathrm{d}\theta \int_0^{2\pi} \mathrm{d}\phi f_{\beta 1} \left|\mathbf{v}_\alpha - \mathbf{v}_{\beta 1}\right| \\ N_{\alpha\beta} &= \tfrac{\sigma_{\alpha\beta}^2}{2} \int_{-\infty}^{+\infty} \mathrm{d}\mathbf{v_1} \int_0^\pi \sin\theta \,\mathrm{d}\theta \int_0^{2\pi} \mathrm{d}\phi f'_\alpha f'_{\beta 1} \left|\mathbf{v}_\alpha - \mathbf{v}_{\beta 1}\right| \end{aligned}\right\}. \tag{8}$$

The distribution functions in the integrands are hereafter taken after the first step (the ~ symbols are omitted).

Using the implicit approach the discretised version of Eq. (7) is presented as:

$$J_{\alpha\beta}^{k,n-1} = -\nu_{\alpha\beta}^{k,n-1} f_\alpha^{k,n} + N_{\alpha\beta}^{k,n-1}, \tag{9}$$

where

$$\left.\begin{aligned} \nu_{\alpha\beta}^{k,n-1} &= \tfrac{\sigma_{\alpha\beta}^2}{2} \int_{-\infty}^{+\infty} \mathrm{d}\mathbf{v_1} \int_0^\pi \sin\theta \,\mathrm{d}\theta \int_0^{2\pi} \mathrm{d}\phi f_{\beta 1}^{k,n-1} \left|\mathbf{v}_\alpha^k - \mathbf{v}_{\beta 1}^k\right| \\ N_{\alpha\beta}^{k,n-1} &= \tfrac{\sigma_{\alpha\beta}^2}{2} \int_{-\infty}^{+\infty} \mathrm{d}\mathbf{v_1} \int_0^\pi \sin\theta \,\mathrm{d}\theta \int_0^{2\pi} \mathrm{d}\phi f_\alpha'^{k,n-1} f_{\beta 1}'^{k,n-1} \left|\mathbf{v}_\alpha^k - \mathbf{v}_{\beta 1}^k\right| \end{aligned}\right\}. \tag{10}$$

Remembering (9) the solution of Eq. (6) is presented as

$$f_\alpha^{k,n} = \frac{\tilde{f}_\alpha^{k,n-1} + \Delta t\left[N_{\alpha\alpha}^{k,n-1} + N_{\alpha\beta}^{k,n-1}\right]}{1 + \Delta t\left[\nu_{\alpha\alpha}^{k,n-1} + \nu_{\alpha\beta}^{k,n-1}\right]}. \tag{11}$$

The calculation of integrals $\nu_{\alpha\beta}^{k,n-1}$ and $N_{\alpha\beta}^{k,n-1}$ in Eq. (9) (see Eq. (10)) turns out to be a major challenge from the point of view of CPU requirements. It is known that the conventional approach to calculation of these integrals leads to a relative error δ of the order of $K^{-1/s}$, where K is the number of cells used in numerical integration, s is the dimension of the integral [32]. This means that in order to perform the integration with the error less than 1% in a 5-dimensional space, one should use at least 10^{10} cells. This is unrealistic in practical applications.

In the suggested algorithm, the conventional approach to the calculation of these integrals is replaced by the integration based on the random cubature formulae. In this case the expressions for $\nu_{\alpha\beta}^{k,n-1}$ and $N_{\alpha\beta}^{k,n-1}$ are rewritten as:

$$\left.\begin{aligned} \nu_{\alpha\beta}^{k,n-1} &= \tfrac{V}{K_0} \tfrac{\sigma_{\alpha\beta}^2}{2} \sum_{l=1}^{K_0} \frac{f_{\beta 1 l}^{k,n-1} |\mathbf{v}_\alpha - \mathbf{v}_{\beta 1 l}| \sin\theta_l}{p(\mathbf{w}_l)} \\ N_{\alpha\beta}^{k,n-1} &= \tfrac{V}{K_0} \tfrac{\sigma_{\alpha\beta}^2}{2} \sum_{l=1}^{K_0} \frac{f_{\alpha l}'^{k,n-1} f_{\beta 1 l}'^{k,n-1} |\mathbf{v}_\alpha - \mathbf{v}_{\beta 1 l}| \sin\theta_l}{p(\mathbf{w}_l)} \end{aligned}\right\}, \tag{12}$$

where V is the volume of the 5-dimensional space, $\mathbf{w}_l \equiv \mathbf{w}_l(\mathbf{v}_{\beta 1 l}, \theta_l, \phi_l)$ is the arbitrary chosen point in this 5-dimensional space (three components of velocity of molecules before collisions and directions of their velocities after collisions), $p(\mathbf{w}_l)$ is the value of the probability density function of the distribution of these points and K_0 is the total number of these points (assumed number of collisions in a given cell in physical and velocity spaces). The summation in Eq. (12) is performed over all these points. The dependence of parameters $v_{\alpha\beta}^{k,n-1}$ and $N_{\alpha\beta}^{k,n-1}$ in (12) on ϕ enters via $f_{\alpha l}^{\prime k,n-1}$ and $f_{\beta 1 l}^{\prime k,n-1}$. Assuming that the choice of $\mathbf{w}_l$ is random, the relative error of calculation of $v_{\alpha\beta}^{k,n-1}$ and $N_{\alpha\beta}^{k,n-1}$ is proportional to $1/\sqrt{K_0}$ and does not depend on the dimension of the space [17,32]. For practical calculations, we assumed homogeneous distribution of $\mathbf{w}_l$, which implies that $p(\mathbf{w}_l) = 1$. This can be justified, keeping in mind the following factors. Firstly, the distribution function of molecules inside the Knudsen layer can differ substantially from the equilibrium one and it is not possible to predict its form before the solution has been found, in the general case. Secondly, when studying the interaction between molecules it is important to take into account not only their numbers but also their kinetic energies. These two circumstances would make it very difficult to justify any other choice of $p(\mathbf{w}_l)$ except $p(\mathbf{w}_l) = 1$.

The practical efficiency of the application of Eq. (12) largely depends on the choice of nodes $\mathbf{w}_l$. One of the most widely used approaches for choosing these nodes is based on the so called Korobov sequences [33,34,17]. Using these sequences instead of random numbers makes it possible to reduce errors of computations. In the case of piecewise constant functions (used in our numerical analysis), the errors of calculations using Korobov sequences are proportional to $1/K_0$ (instead of $1/\sqrt{K_0}$ when random numbers are used; see above). The condition $p(\mathbf{w}_l) = 1$ for these sequences is satisfied. This approach is used in our algorithm.

The explicit expression for V can be presented as:

$$V = 2\pi^2 |v_{x(\max)} - v_{x(\min)}||v_{y(\max)} - v_{y(\min)}||v_{z(\max)} - v_{z(\min)}|. \tag{13}$$

As mentioned in Section 2, the modelling of the collision processes is based on the assumption that the collisions are elastic (momentum and energy are conserved) and the directions of velocities of molecules in the coordinate system linked with their centres of inertia are random. The numerical implementation of this model, however, is linked with a number of difficulties. These are related to the fact that randomly chosen directions of molecular velocities after collisions are likely to lead to the values of these velocities lying between the values in the nodes of the discretised velocity space. This eventually can lead to non-conservation of impulses and energies during the collision processes. In the early papers, this problem was resolved by introducing the correction of the distribution function after the collisions [17]. Although these corrections made the system conservative, they led to additional sources of errors. In the projection method, developed later in [20,21,27,29], the actual molecular velocities after collisions were replaced by pairs of velocities referring to the nearest nodes. These velocities were taken with appropriate weights, which ensured that the conservation of impulses and energies took place during individual collisions. This, however, led to increase of the complexity of the algorithm.

The approach used in our algorithm is different from the ones described above. It is based on the discretisation of the velocities not only during the description of molecular motion but also in the analysis of the collision processes, shown schematically in Fig. 1. Two colliding molecules enter a certain zone of interaction with velocities $\mathbf{v}$ and $\mathbf{v}_1$. We do not know the details of the collision process but we assume that after the collision these molecules acquire new velocities $\mathbf{v}'$ and $\mathbf{v}_1'$ which satisfy the following conditions:

(1) The total impulse and energy of both molecules are conserved (collisions are elastic);
(2) Vectors $\mathbf{v}'$ and $\mathbf{v}_1'$ belong to an a priori chosen set of velocities.

The second assumption was not used in the original method developed in [17]. The idea that molecular velocities after collisions can be chosen among the nodes in the velocity space, similarly to the choice of velocities before collisions, is not new. For example, a conservative scheme based on a special choice of collision parameters was suggested and developed in [35–37]. In this scheme, the velocity vectors of molecules before and after collisions were taken in the nodes of the originally discretised velocity space. Our approach has some similarities with the approaches used in [35–37] but the details are different. Its practical application can be best illustrated if we consider the collision process in the frame of reference linked with the centre of inertia of both molecules and describe the system dynamics in terms of impulses rather than velocities. In this frame of

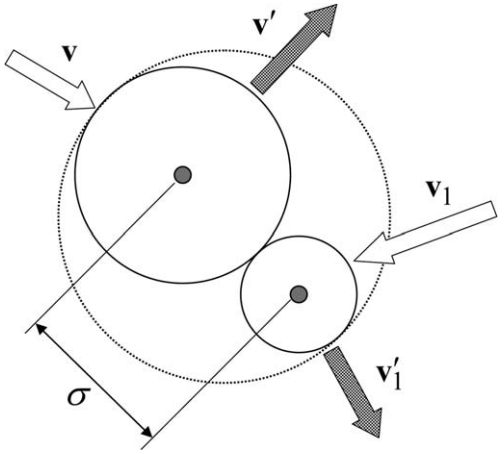

Fig. 1. Scheme of the collision process between two molecules. $\mathbf{v}$ and $\mathbf{v}_1$ are velocities of molecules before the collision; $\mathbf{v}'$ and $\mathbf{v}'_1$ are their velocities after the collision. σ is the sum of radii of these molecules.

reference, the impulses of oncoming molecules have equal values but opposite directions. For the two dimensional case, these are schematically shown in Fig. 2a and b. In the case shown in Fig. 2a, $p_{cx} = 0$ and $p_{cy} = \Delta p$, where the subscript $_c$ indicates that the component of the impulse is taken in the frame of reference linked with the centre of inertia of both molecules, Δp is the grid size in the impulse space (assumed to be the same in all directions). In the case shown in Fig. 2b, $p_{cx} = -\Delta p$ and $p_{cy} = 2\Delta p$. The collision process leads to the rotation of impulses of both molecules in such a way that their absolute values remain the same but the directions opposite. All the possible impulses satisfying these conditions, lie on the circumferences shown in Fig. 2a and b.

In the general case, it can be shown that all components of impulses in the frame of reference linked with the centre of inertia of colliding molecules should be integers of $0.5\Delta p$. In the two-dimensional case shown in Fig. 2a and b, these correspond to the points of intersection of the circumference with the nodes in the impulse space. In the case shown in Fig. 2a, there are 4 such points corresponding to 4 various combinations of impulses of molecules after collisions. In the case shown in Fig. 2b, the number of such points increases to 8. This number of intersection points appears to be maximal. The increase of the radius of the circle would lead to the situation when the circumference approaches very closely to additional nodes on the velocity grid but these nodes would not lie on the circumference itself (this is the result of our observation, although we were not able to proove this rigorously). In the three dimensional case, the circumferences shown in

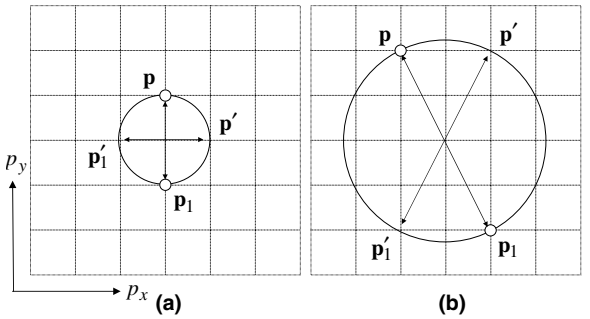

Fig. 2. Scheme of the collision process between two molecules in the frame of reference linked with their centre of inertia. $\mathbf{p}$ and $\mathbf{p}_1$ are impulses of molecules before the collision; $\mathbf{p}'$ and $\mathbf{p}'_1$ are their impulses after the collision. Subscripts $_c$ indicating the centre of inertia are omitted. All impulses lie in the plane (p_x, p_y). The sizes of the grid in this plane are assumed to be the same in p_x and p_y directions and equal to Δp. Both components of all four vectors $\mathbf{p}$, $\mathbf{p}_1$, $\mathbf{p}'$ and $\mathbf{p}'_1$ are integers of $0.5\Delta p$. The absolute values of these vectors are equal to the radii of the corresponding circumferences.

Fig. 2a and b turn into the surfaces of spheres and the maximal number of possible intersection points increases to 24. This corresponds to the maximal total number of combinations of impulses after collisions which equals 24. This number of combinations is relatively small. Hence, in the practical implementation of this model, the calculations of the right hand sides of Eq. (12) were performed for all possible values of θ and ϕ for each collision and then the results were averaged over these variables. This is expected to improve the accuracy of the results compared with the random choice of θ and ϕ from the set of possible values of these variables.

We believe that this new approach to finding θ and ϕ after the collisions provides consistency in discretisation processes used for the description of molecular dynamics and collision processes. It was tested on numerous problems, some of which will be discussed in Section 5.

4. Knudsen layer

The numerical solution of the Boltzmann equation, using the model and the numerical algorithm discussed in Sections 2 and 3, allows us to describe mass and heat transfer processes in binary systems with high level of accuracy. The practical application of this model and numerical algorithm, however, requires the specification of boundary conditions. This sometimes leads to additional complications. For example, in the case of modelling of the droplet evaporation process into a sufficiently dense air, the region around the droplet is usually subdivided into two regions: Knudsen layer and hydrodynamic region (cf. [10]). Heat and mass transfer in the former are studied based on the kinetic model, while in the latter they are studied based on the hydrodynamic model. Since the thickness of the Knudsen layer δ_{Kn} is usually much less than the droplet radius, the curvatures of the droplet surface and the outer boundary of the Knudsen layer can be ignored. The scheme of the processes involved is schematically shown in Fig. 3. Note that the term 'Knudsen layer' in our analysis refers to a two-surface problem.

The boundary conditions at the droplet surface ($x = 0$) for both fuel vapour and air molecules are assumed to take the form:

$$f_{\mathrm{as,bs}}(x = 0, v_x > 0) = n_{\mathrm{as,bs}} \left(\frac{1}{2\pi R_{\mathrm{a,b}} T_{\mathrm{s}}} \right)^{3/2} \exp\left(- \frac{v_x^2 + v_y^2 + v_z^2}{2 R_{\mathrm{a,b}} T_{\mathrm{s}}} \right), \tag{14}$$

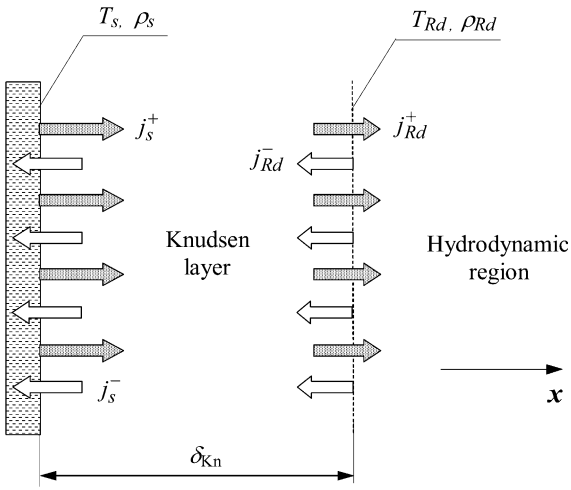

Fig. 3. Scheme of mass fluxes of molecules in the Knudsen layer during the evaporation process. j_{s}^+ is the flux leaving the surface of the droplet; j_{s}^- is the return flux to the surface of the droplet; $j_{\mathrm{Rd}} = j_{\mathrm{Rd}}^+ - j_{\mathrm{Rd}}^-$ is the net flux leaving the outer boundary of the Knudsen layer and entering the hydrodynamic region. T_{s} and T_{Rd} are temperatures at the surface of the droplet and at the outer boundary of the Knudsen layer respectively. ρ_{s} is the fuel vapour density corresponding to T_{s}, ρ_{Rd} is the fuel vapour density at the inner boundary of the hydrodynamic region. δ_{Kn} is the thickness of the Knudsen layer.

where $n_{as,bs} = \rho_{as,bs}/m_{a,b}$ are number densities of molecules a and b (fuel vapour and air), $R_{a,b}$ are the corresponding gas constants. ρ_{as} is the density of the saturated vapour corresponding to the droplet surface temperature T_s. The values of n_{bs} are determined from the equality of incident and reflected fluxes at the droplet surface. x-axis is perpendicular to the droplet surface. A more general form of the boundary condition for the Boltzmann equation at the solid surface was considered in [38].

Not all vapour molecules leaving the droplet surface reach the ambient gas. Some of them eventually form a return flux j_s^- as shown in Fig. 3, so that the outward flux at the outer boundary of the Knudsen layer j_{Rd}^+ is less than j_s^+. This leads to the situation when the vapour density at this boundary is less than ρ_s. As in the case of the outward fluxes from the droplet surface, the return fluxes from the outer boundary of the Knudsen layer are assumed Maxwellian for both types of molecules:

$$f_{aRd,bRd}(x = \delta_{Kn}, v_x < 0) = n_{aRd,bRd}\left(\frac{1}{2\pi R_{a,b}T_{Rd}}\right)^{3/2}\exp\left(-\frac{v_x^2 + v_y^2 + v_z^2}{2R_{a,b}T_{Rd}}\right), \tag{15}$$

where $n_{aRd,bRd}$ are mass densities of fuel vapour and air molecules at the inner boundary of the hydrodynamic region, T_{Rd} is the temperature at the outer boundary of the Knudsen layer. The value of T_{Rd} is assumed to be equal to the corresponding value at the inner boundary of the hydrodynamic region.

In most practical applications, T_{Rd} is close to T_s, and it is assumed that $T_{Rd} = T_s$. Matching of $j_{Rd} = j_{Rd}^+ - j_{Rd}^-$ and the diffusion flux in the hydrodynamic region j_{diff} leads to the additional boundary condition at the outer boundary of the Knudsen layer (cf. the corresponding matching conditions used in [10]).

One of the main obstacles in practical implementation of this approach to kinetic modelling of droplet evaporation into numerical codes, lies in the uncertainty of the value of the thickness of the Knudsen layer δ_{Kn}. If this thickness is assumed too large, then CPU requirements would be too large for practical applications. If this thickness is assumed too small, then the outward mass flux at the outward boundary of the Knudsen layer could have been grossly overestimated. To illustrate the nature of the problem, let us consider a specific example of evaporation of n-dodecane ($C_{12}H_{26}$) droplet, which can be a good approximation of a diesel fuel droplet. We took $T_s = 600$ K, $\rho_s(T_s) = 22.09$ kg/m^3 (this is determined by the Clausius Clapeyron equation for the saturated fuel vapour pressure) and assumed that no air is present in the Knudsen layer. We took $\delta_{Kn} = 50\lambda_c$, where λ_c is the mean free path of fuel vapour molecules calculated for the vapour's temperature T_s and density ρ_s as specified above. Also, we assumed that $\rho_{Rd} = 0.8\rho_s$. Using these boundary conditions and the model with numerical algorithm described in Sections 2 and 3, we calculated the plots of ρ/ρ_s versus x/λ_c, where $\rho = \rho(x)$ is the density of fuel vapour in the Knudsen layer and x is the distance from the droplet surface. The results are shown in Fig. 4 for x/λ_c in the range from 0 to 10.

As follows from Fig. 4, the values of ρ/ρ_s remain practically the same at $x > 5\lambda_c$. This means that we would be able to obtain the same result if the thickness of the Knudsen layer is decreased by a factor of 10. In this case, the choice of the value of δ_{Kn} turns out to be a relatively simple task. Note that the fuel vapour density jump is observed both at the droplet surface and at the outer boundary of the Knudsen layer. This is a typical result following from the kinetic modelling of the phenomena (cf. [39]). The results shown in Fig. 4 are not self-consistent, as the value of ρ_{Rd} (following from the condition of matching fluxes at the outer boundary

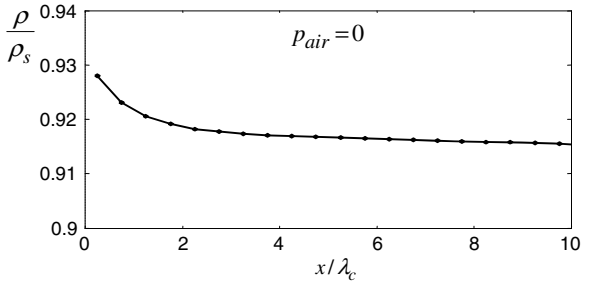

Fig. 4. Plots of normalised density of fuel vapour ρ/ρ_s versus normalised distance from the droplet surface x/λ_c for x/λ_c in the range from 0 to 10, assuming that $T_s = T_{Rd} = 600$ K, $\rho_{Rd} = 0.8\rho_s$, $\delta_{Kn} = 50\lambda_c$ and the partial pressure of air in the Knudsen layer is equal to zero. λ_c is the mean free path of vapour molecules calculated at $T = T_s$ and $\rho = \rho_s(T_s)$.

of the Knudsen layer and the hydrodynamic region) cannot be imposed externally. Hence, the iterations would be required to establish the true value of ρ_{Rd}.

The situation becomes rather different when the presence of air in the Knudsen layer is taken into account. The plots of ρ/ρ_s versus x/λ_c for the same boundary conditions for vapour as in Fig. 4 are shown in Fig. 5. The partial pressure of air is equal to 2 and 30 bar and various δ_{Kn}/λ_c (indicated near the plots) were used. As can be seen from this figure, the presence of air leads to a number of important effects. The reductions of the density jumps at the droplet surface and at the outer boundary of the Knudsen layer are the expected ones (cf. [39]). A more interesting result is the dependence of ρ/ρ_s on the chosen values of δ_{Kn} for both partial pressures of air. No saturation effect demonstrated in Fig. 4 can be seen in this case. From the point of view of the underlying physics, this can be related to the fact that additional collisions lead to a more homogeneous drop of fuel vapour density across the Knudsen layer. From the point of view of practical applications, this leads to the problem of correct choice of δ_{Kn}. A possible approach to this problem would be to take the largest possible value of δ_{Kn}. However, there would be no guarantee that this would allow us to reach the saturation level. Also, the increase of this thickness 10 times would lead to increase of the required CPU time by a factor of 100, which would make this approach not practical.

We suggest an alternative approach to this problem focused on the direct finding of vapour density at the inner boundary of the hydrodynamic region (ρ_{Rd}), rather than estimation of the thickness of the Knudsen layer. This approach is based on the observation that the actual flux of vapour leaving the droplet can be found from the relation:

$$j_s = j_s^+ - j_s^-, \tag{16}$$

where j_s^+ is the flux in the x direction which is determined by T_s and $\rho_s(T_s)$, j_s^- is the flux in the $-x$ direction. The latter is formed due to the fact that molecules of vapour emitted from the surface of the droplet collide

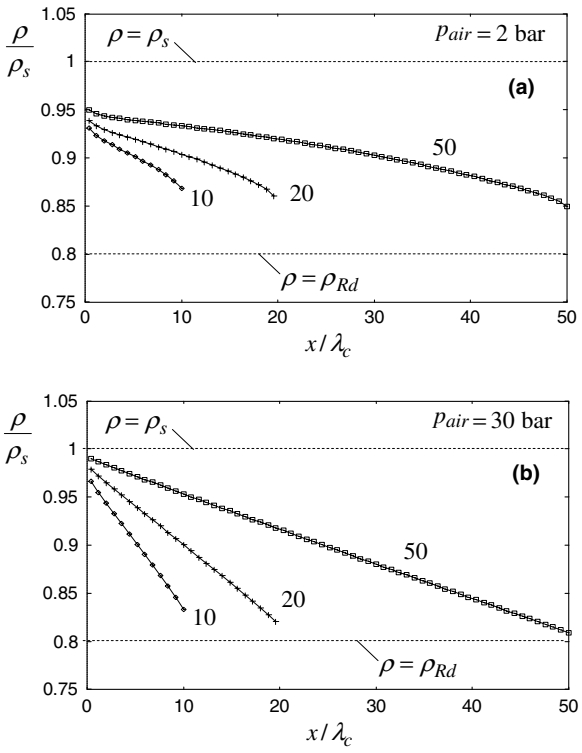

Fig. 5. The same as Fig. 4 but for the cases when air is present in the Knudsen layer (a: $p_{air} = 2$ bar; b: $p_{air} = 30$ bar) and various values of δ_{Kn}/λ_c (numbers near the curves).

between themselves and other molecules and part of them return to the droplet. The value of j_s^- is not directly related to T_s and ρ_s. It is found from the direct numerical solution of the Boltzmann equation for the vapour.

The net mass flux of the vapour at an arbitrary distance from the droplet surface within the Knudsen layer can be found from the relation:

$$j = j^+ - j^-. \tag{17}$$

Both j^+ and j^- decrease with increasing distance from the droplet surface (x) but the value of j remains equal to j_s due to the conservation of mass. A decrease of j due to the curvature of the droplet surface is taken into account in due course.

The plots of j^+ and j^- for vapour versus x/λ_c for the same values of parameters as in Fig. 5 and $p_{air} = 2$ bar are shown in Fig. 6a. As follows from this figure, both j^+ and j^- decrease with increasing x/λ_c but the difference between them (j: net flux) remains the same as expected. The same plots as in Fig. 6a but for air are shown in Fig. 6b. As follows from the latter figure, both j^+ and j^- for air increase with increasing x/λ_c but the difference between them remains close to zero. This reflects the fact that there is no net flux of air towards droplets in steady state conditions. A small difference between j^+ and j^- for air (about 1%) reflects a small error in computations. There is no underlying physics behind this difference.

When the Knudsen layer is thin enough, then the number of collisions in it is expected to be small and the mass flux of reflected molecules (j_s^-) is close to zero. Hence, $j \approx j_s \approx j_s^+$. The increase of δ_{Kn} leads to the increase of j_s^- and the corresponding decrease of j_s. However, at large distances from the droplet surface the effects of collisions on the returning flux diminishes and j_s^- reaches its saturation level. In this case, the constant flux of vapour $j \approx j_s \approx j_{Rd}$ is established.

Also, inspection of Fig. 5 shows us that the value of δ_{Kn} affects the distribution of vapour density inside the Knudsen layer. Let ρ_1 and ρ_2 be vapour densities near the droplet surface and near the outer boundary of the Knudsen layer. As mentioned earlier, $\rho_1 < \rho_s$, $\rho_2 > \rho_{Rd}$ and $\rho_1 > \rho_2$. The latter inequality results from molecular collisions. In the absence of such collisions (free molecular flow) $\rho_1 = \rho_2$. In this case the values

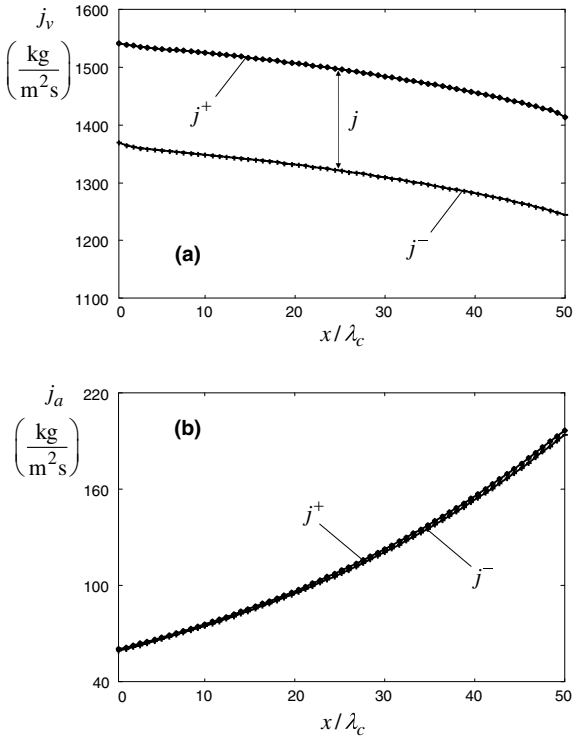

Fig. 6. Plots of j^+ and j^- versus x/λ_c for vapour (a) and air (b). The values of input parameters T_s, ρ_{Rd} and λ_c are the same as for Fig. 5. The partial pressure of air is equal to 2 bar.

of $\rho_s - \rho_1$ and $\rho_2 - \rho_{Rd}$ would reach their maximum values. In the case of large number of collisions, gas behaves similarly to continuous medium where ρ_1 is close to ρ_s, ρ_2 is close to ρ_{Rd} and the gradient of ρ inside the Knudsen layer reaches its maximal value.

We would expect that $\Delta\rho \equiv \rho_1 - \rho_2$ depends on the number of collisions experienced by a molecule of vapour inside the Knudsen layer $N = \delta_{Kn}/\lambda_c$ and varies between 0 and $\rho_s - \rho_{Rd}$ when N increases from 0 to ∞.

Plots of j and $\Delta\rho$ versus N for the same values of parameters as in Fig. 5a are shown in Fig. 7a and b. The observation of these figures shows that they are almost symmetric. This allows us to present the expressions for j and $\Delta\rho$ as:

$$\left.\begin{aligned} j &= AF(N) + B \\ \Delta\rho &= CF(N) + D \end{aligned}\right\}, \tag{18}$$

where A,B,C,D are constants, $F(N)$ is an unknown function of N. In this case, j is a linear function of $\Delta\rho$:

$$j = -a\Delta\rho + b, \tag{19}$$

where a, b are new constants depending on T_s and the partial pressure of air. The negative value of the coefficient before $\Delta\rho$ reflects the fact that j decreases when $\Delta\rho$ increases.

The predictions of Eq. (19) have been checked against the results of numerical solutions of the Boltzmann equations for air partial pressures in the range from 2 atm to 50 atm, $T_s = 600$ K, $\rho_{Rd} = 0.8\rho_s$ and $\rho_s(T_s) = 22.09$ kg/m^3 (assuming that the vapour is that of n-dodecane). The results are shown in Fig. 8. The points connected by solid lines correspond to various values of δ_{Kn} in the range between $5\lambda_c$ and $100\lambda_c$ ($\delta_{Kn}/\lambda_c = 10,50,100$ for $p_{air} = 2$ bar; $\delta_{Kn}/\lambda_c = 10,20,50$ for $p_{air} = 10$ bar and $p_{air} = 25$ bar; $\delta_{Kn}/\lambda_c = 5$, 10, 20 for $p_{air} = 50$ bar). The dotted lines are extrapolations of the solid ones. The limiting point for all these lines refers to $\Delta\rho_{max} = 4.42$ kg/m^3. This figure clearly confirms the validity of Eq. (19). The practical application of this figure, however, is limited as all plots on it refer to $\rho_{Rd} = 0.8\rho_s$.

In the plots shown in Fig. 9, we restricted our analysis to just one value of $p_{air} = 30$ bar but considered a set of values of ρ_{Rd} in the range form $0.6\rho_s$ to $0.8\rho_s$. As can be seen from this figure, j is clearly a linear function of

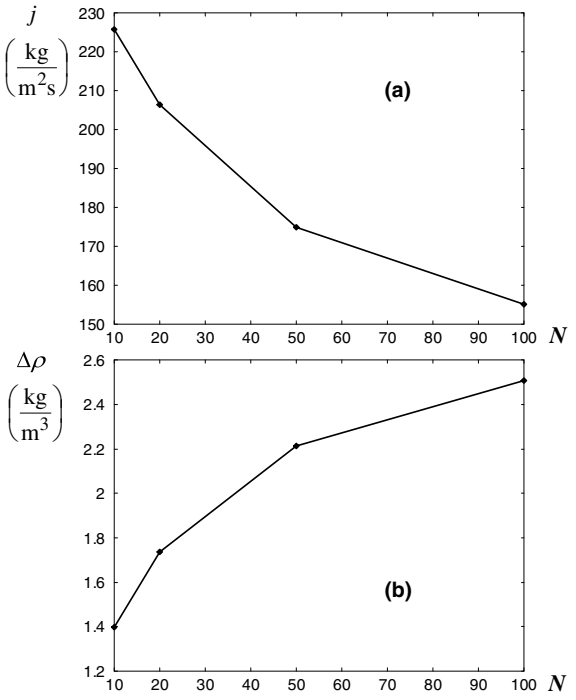

Fig. 7. Plots of j versus N (a) and $\Delta\rho$ versus N (b) for the same values of parameters as in Fig. 5a.

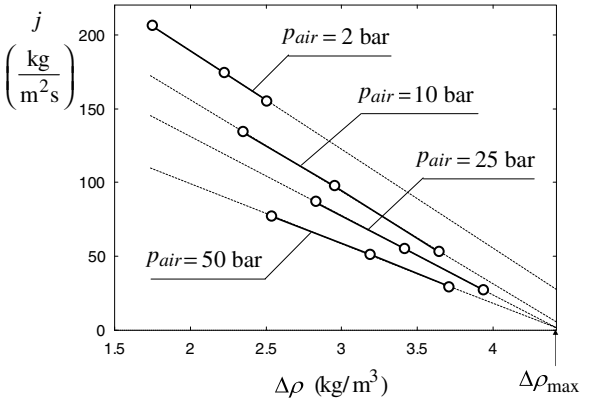

Fig. 8. Plots of j versus $\Delta\rho$ for $T_s = T_{Rd} = 600$ K, $\rho_{Rd} = 0.8\rho_s$, $\rho_s(T_s) = 22.09$ kg/m^3 and partial air pressures from 2 bar to 50 bar (indicated near the lines). The values of j and $\Delta\rho$ used for these plots were calculated for the values of δ_{Kn} in the range between $5\lambda_c$ and $100\lambda_c$ ($\delta_{Kn}/\lambda_c = 10,50,100$ for $p_{air} = 2$ bar; $\delta_{Kn}/\lambda_c = 10,20,50$ for $p_{air} = 10$ bar and $p_{air} = 25$ bar; $\delta_{Kn}/\lambda_c = 5,10,20$ for $p_{air} = 50$ bar). λ_c was calculated at $T = T_s$ and $\rho = \rho_s(T_s)$.

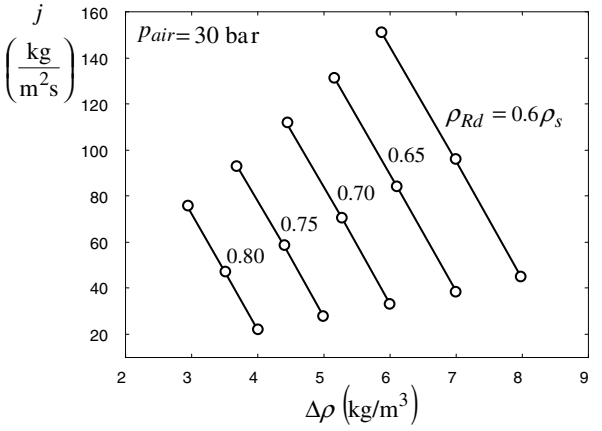

Fig. 9. Plots of j versus $\Delta\rho$ for $T_s = T_{Rd} = 600$ K, $\rho_s(T_s) = 22.09$ kg/m^3, partial air pressure 30 bar and various ρ_{Rd} (numbers near the lines). The values of j and $\Delta\rho$ used for these plots were calculated for $\delta_{Kn} = 10\lambda_c$, $\delta_{Kn} = 20\lambda_c$, $\delta_{Kn} = 50\lambda_c$. λ_c was calculated at $T = T_s$ and $\rho = \rho_s(T_s)$.

$\Delta\rho$ in agreement with Eq. (19). The same results were obtained for other values of T_s in the range from 400 K to 659 K (critical temperature of n-dodecane).

The plots shown in Figs. 8 or 9 are extrapolated towards higher $\Delta\rho$ and their intersections with the vertical lines corresponding to $\Delta\rho = \Delta\rho_{max}$ are found. This is expected to give a true value of j_{Rd} for the chosen value of ρ_{Rd}, since $\Delta\rho$ cannot exceed $\Delta\rho_{max}$. Explicit expression for j can be obtained from Eq. (19) by replacing $\Delta\rho$ by $\Delta\rho_{max} = \rho_s - \rho_{Rd}$ in it:

$$j_{Rd} = -a(\rho_s - \rho_{Rd}) + b(\rho_{Rd}), \tag{20}$$

where we explicitely indicated that b is a function of ρ_{Rd}. Note that in the limiting case when $\rho_{Rd} = \rho_s$ the net flux j_{Rd} in expected to be zero. Hence, $b|_{\rho_{Rd}=\rho_s} = 0$. In the general case from our computations (see Fig. 9), it follows that b is proportional to $\rho_s - \rho_{Rd}$, i.e. $b = c(\rho_s - \rho_{Rd})$, where c is the new constant. This allows us to rewrite Eq. (20) as:

$$j_{Rd} = -a_1(\rho_s - \rho_{Rd}), \tag{21}$$

where $a_1 = a - c$. Eq. (21) indicates that j_{Rd} is the linear function of ρ_{Rd}.

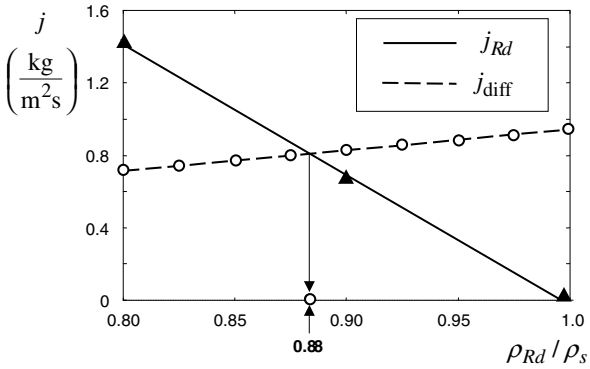

Fig. 10. Plots of j versus $\rho_{\mathrm{Rd}}/\rho_{\mathrm{s}}$, as obtained from Fig. 9, and j_{diff} versus $\rho_{\mathrm{Rd}}/\rho_{\mathrm{s}}$, as obtained from the mass diffusion and convection equation in the hydrodynamic region (Eq. (22)). The intersection point between these two curves gives the value of $j = j_{\mathrm{diff}} \approx 0.81$ kg/(m^{2}s) and $\rho_{\mathrm{Rd}} \approx 0.88\rho_{\mathrm{s}}$.

Using Eq. (21) or the set of lines shown in Fig. 9, we obtained $j_{\mathrm{Rd}}(\Delta\rho_{\max})$ and presented the plot of $j_{\mathrm{Rd}}(\rho_{\mathrm{Rd}}/\rho_{\mathrm{s}})$ (this is the true vapour flux as predicted by the kinetic model). Also, we obtained the corresponding plot $j_{\mathrm{diff}}(\rho_{\mathrm{Rd}}/\rho_{\mathrm{s}})$ as predicted by the conventional diffusion theory applicable in the hydrodynamic regime [14]:

$$j_{\mathrm{diff}} = \frac{\rho_{\mathrm{mix}} D_{\mathrm{c}}}{R_{\mathrm{d}}} \ln(1 + B_M), \tag{22}$$

where B_M is the Spalding mass number defined as:

$$B_M = \frac{Y_{\mathrm{fRd}}}{1 - Y_{\mathrm{fRd}}}, \tag{23}$$

$Y_{\mathrm{fRd}} = \rho_{\mathrm{Rd}}/\rho_{\mathrm{mix}}$, ρ_{mix} is the density of the mixture of vapour and air, D_{c} is the diffusion coefficient of vapour in air. When deriving Eq. (22) we ignored the difference of areas of the droplet surface and the outer boundary of the Knudsen layer.

The plots of j_{Rd} versus $\rho_{\mathrm{Rd}}/\rho_{\mathrm{s}}$ and j_{diff} versus $\rho_{\mathrm{Rd}}/\rho_{\mathrm{s}}$ for the same values of parameters as in Fig. 9 are shown in Fig. 10. The intersection between these two curves gives the true values of ρ_{Rd} and $j = j_{\mathrm{Rd}} = j_{\mathrm{diff}}$. It follows from Fig. 10, that these values are: $j = 0.81$ kg/(m^{2}s) and $\rho_{\mathrm{Rd}} = 0.88\rho_{\mathrm{s}}$.

5. Applications

5.1. Relaxation of the non-equilibrium distribution function

Let us consider a spatially homogeneous air at atmospheric pressure and average temperature 300 K. Its distribution function is approximated by the sum of two shifted Maxwellian distributions:

$$f = \left(\frac{n_1}{2\pi R_{\mathrm{air}} T_1}\right)^{3/2} \exp\left(-\frac{(v_x - v_{01})^2 + v_y^2 + v_z^2}{2R_{\mathrm{air}} T_1}\right) + \left(\frac{n_2}{2\pi R_{\mathrm{air}} T_2}\right)^{3/2} \exp\left(-\frac{(v_x + v_{02})^2 + v_y^2 + v_z^2}{2R_{\mathrm{air}} T_2}\right), \tag{24}$$

where $n_1/n_2 = 2$, $T_2/T_1 = 0.75$.

The plot of f versus v_x and v_y, as predicted by Eq. (24), is shown in Fig. 11a. Our task is to calculate the time evolution of this distribution function. Since the distribution is assumed to be initially spatially homogeneous, it will remain spatially homogeneous at any other $t > 0$. In this case, there is no need to consider the displacement of molecules in the physical space and the attention can be concentrated on the changes of f due to collision processes. Our calculations predict gradual smoothening of f (see Fig. 11b and c) and its final evolution into the Maxwellian distribution (Fig. 11d). The average temperature and the total number of molecules remain the same during this evolution. The time interval between the distributions shown in Fig. 11a and d is about 0.005 μs. This result is consistent with the qualitative analysis of this process and can be considered as a reliable functionality test for the new algorithm.

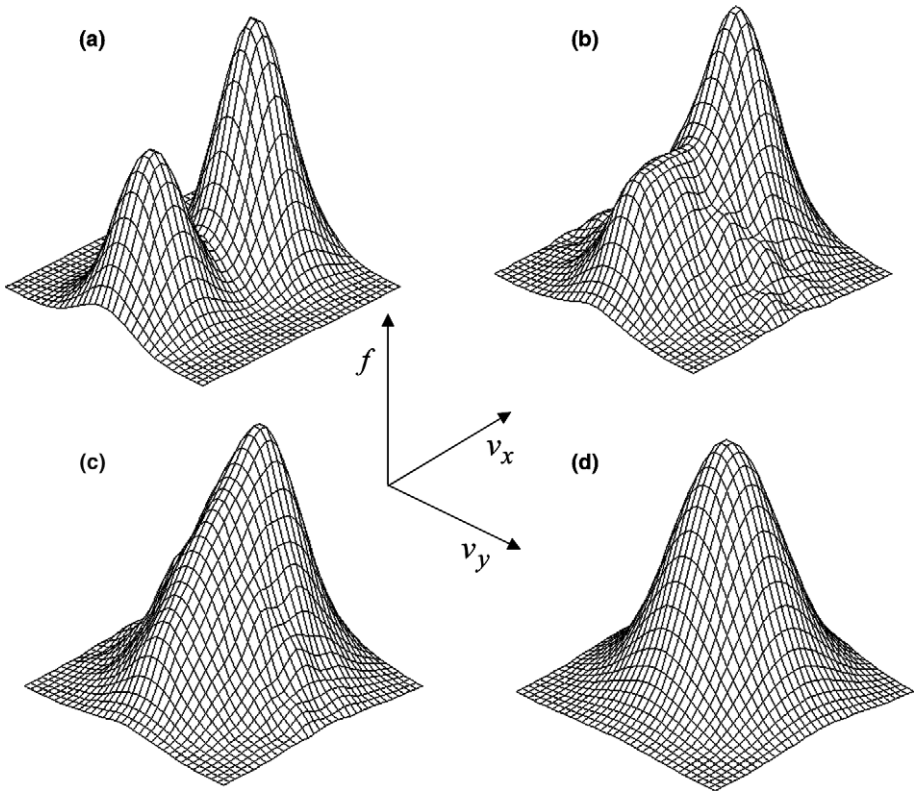

Fig. 11. The plots of f versus (v_x, v_y) as predicted by Eq. (24) (a) and the evolution of f with time during the first 0.005 μs (b–d). The average temperature is assumed equal to 300 K and the pressure is assumed equal to 1 bar. Spatial homogeneity of gas is assumed.

5.2. Evaporation and condensation in the presence of inert gas

The next problem to be considered is identical to the one studied in [23]. This problem focuses on the analysis of the mixture of vapour with molecular concentration n_A and inert gas with molecular concentration n_B confined between two infinite plates located at $x = 0$ and $x = L$ as shown in Fig. 12. The temperature at the surface of the first plate is assumed to be equal to T_I. The concentration of evaporating molecules n_I at this plate is determined by the saturation condition at $T = T_I$, while molecular concentration at the second boundary is maintained equal to $n_{II} = 2\,n_I$. The temperature at the surface of the second plate is equal to that at the first: $T_I = T_{II}$. The initial concentrations of the vapour and inert gas are assumed to be homogeneous and equal to n_I and $0.5n_I$ respectively in the whole domain. The results obtained for the steady state conditions practically do not depend on the choice of the initial distribution of vapour. The average concentration of the inert gas is assumed to be conserved. We assumed that the diameters and masses of all molecules are

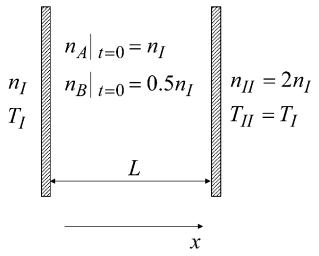

Fig. 12. Boundary and initial conditions for the evaporation and condensation problem discussed in Section 5.2.

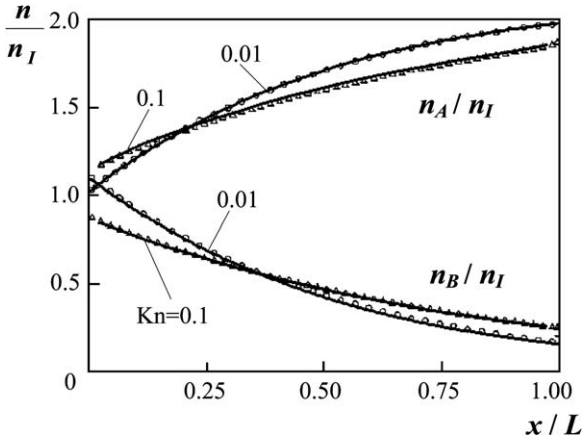

Fig. 13. Plots of n_A/n_I versus x/L and n_B/n_I versus x/L as obtained in [23] for $Kn = 0.1$ (triangles) and $Kn = 0.01$ (circles). The same plots obtained using the model and numerical algorithm described in Sections 2–4 (solid curves).

the same and equal to those of N_2, although the results would not change for other values of these parameters provided that they are the same for vapour and inert gas (see [23]). The initial distribution functions of both vapour and inert gas are assumed to be Maxwellian.

The authors of [23] studied the time evolution of the system described above using the standard direct simulation Monte-Carlo (DSMC) method by Bird [15,16]. They demonstrated that this system asymptotically approaches to the steady state spatial distribution of concentrations of vapour $n_A(x)$ and the inert gas $n_B(x)$. These steady state distributions depend on the values of $Kn = \lambda_c/L$, where the value of the mean free path λ_c for vapour is taken for $T = T_I$ and $n = n_I$. Results of their calculations for $n_A(x)/n_I$ and $n_B(x)/n_I$, for $Kn = 0.1$ and $Kn = 0.01$ are shown in Fig. 13. Triangles refer to $Kn = 0.1$, while circles refer to $Kn = 0.01$. The results of calculations using the model and numerical algorithm described in Sections 2–4 and the same values of parameters as in [23] are shown in the same figure by solid curves. Exceptionally good agreement between the results reported in [23] and those obtained using our algorithm can support the validity of the results obtained by two different algorithms. Note that the agreement between these results was first reported in [28], where the results were presented in a slightly different format.

5.3. Evaporation of a diesel fuel droplet

In this section a realistic problem of evaporation of a diesel fuel droplet into air at total pressure 30 bar is considered. The calculations were performed using the model and numerical algorithm described above and

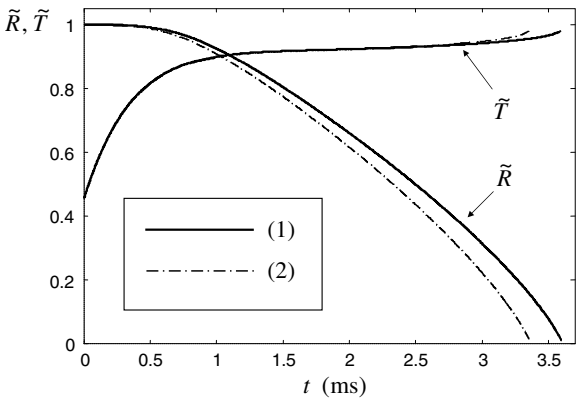

Fig. 14. Plots of $\tilde{R} = R_d/R_{d0}$ versus time and $\tilde{T} = T_s/T_{cr}$ versus time as predicted by the kinetic (1) and hydrodynamic (2) models. $R_{d0} = 5$ μm, $T_g = 650$ K and $T_{cr} = 659$ K.

the hydrodynamic model (see Eq. (22) with $\rho_{Rd} = \rho_s$). The contribution of air in the Knudsen layer is taken into account. Plots of $\tilde{R} = R_d/R_{d0}$ and $\tilde{T} = T_s/T_{cr} = T_s/659$ versus time for $R_{d0} = 5$ μm, $T_{s0} = 300$ K and ambient air temperature $T_{air} = 650$ K are shown in Fig. 14. As follows from this figure, the hydrodynamic model always overpredicts the value of droplet surface temperature and underpredicts the values of droplet radii and the evaporation times as expected. For example, the evaporation time is underpredicted by the hydrodynamic model by about 7%. A similar analysis was performed for $R_{d0} = 20$ μm, and for both R_{d0} for $T_{air} = 750$ K and $T_{air} = 1000$ K. The qualitative trends of all the curves turned out to be the same as shown in Fig. 14. The underprediction of the evaporation time by the hydrodynamic model for other values of the input parameters varied between about 1% and 4%. This result is consistent with the conclusion made in [14] based on the approximate solution of the Boltzmann equation.

Note that the predictions of the kinetic model, described in this paper, would almost coincide with those of the hydrodynamic model if the contribution of air in the Knudsen layer has not been taken into account. Hence, taking into account the presence of air is essential for correct quantitative analysis of fuel droplet heating and evaporation.

6. Conclusions

A numerical algorithm for kinetic modelling of droplet evaporation processes is suggested. This algorithm is focused on the direct numerical solution of the Boltzmann equations for two gas components: vapour and air. The collisions between vapour molecules, air molecules, and air and vapour molecules are taken into account. This numerical algorithm is essentially based on the scheme suggested by Aristov and Tcheremissine [17]. Following this scheme, the physical and velocity spaces are discretised, as in the conventional structured computational fluid dynamics (CFD) codes and the Boltzmann equations are presented in discretised forms. The solution of these discretised equations is performed in two steps. Firstly, molecular displacements are calculated ignoring the effects of collisions. Secondly, the collisional relaxation is calculated under the assumption of spatial homogeneity. The numerical solution of the discretised equations at the first step is performed following the explicit approach. At the second step, the conventional approach to calculating collision integrals is replaced by the integration based on the random cubature formulae. The distribution of molecular velocities after collisions is found based on the assumption that the total impulse and energy of colliding molecules are conserved. The directions of molecular impulses after the collisions are random but their components belong to an a priori chosen set.

A new method of finding the matching conditions for vapour mass fluxes at the outer boundary of the Knudsen layer of evaporating droplets and at the inner boundary of the hydrodynamic region is suggested. This method is based on the observation that the net mass flux of evaporating molecules j is proportional to the difference in fuel vapour densities near the surface of droplets and the outer boundary of the Knudsen layer ($\Delta\rho$). Thus, instead of calculating the value of the mass flux for an actual thickness of the Knudsen layer (which is not known), these fluxes are calculated taking this thickness smaller that the actual one. Then the plots of j versus $\Delta\rho$ are extrapolated to $\Delta\rho_{max}$, where $\Delta\rho_{max} = \rho_s - \rho_{Rd}$ is the maximal possible value of $\Delta\rho$. The value of ρ_{Rd} is found via matching j and the corresponding diffusion flux in the hydrodynamic region.

The numerical algorithm described above is applied to the analysis of three problems. The first problem is the relaxation of initially non-equilibrium distribution function of air molecules towards the Maxwellian one, assuming that there are no spatial gradients in the system. This is essentially a functionality test of the algorithm. The second problem is identical to the one studied in [23]. This problem focuses on the analysis of the mixture of vapour and inert gas confined between two infinite plates. Masses and diameters of vapour and inert gas molecules are assumed to be the same. Results of calculations reported in [23] for $Kn = 0.1$ and $Kn = 0.01$ are compared with the results of calculations using the numerical algorithm described above and the same values of parameters as in [23]. Exceptionally good agreement between the results reported in [23] and those obtained using our algorithm can support the validity of both results and the correctness of both algorithms. The third problem focuses on the modelling of evaporation of diesel fuel droplets into a high pressure air. This problem is similar to the one considered in [14] using an approximate solution of the Boltzmann equation. Using the values of parameters typical for diesel engines (total pressure 30 bar; ambient air temperature 650 K) and taking into account the contribution of air in the Knudsen layer, it was shown that the

kinetic effects predicted by our numerical algorithm are noticeable and need to be taken into account in the analysis of droplet heating and evaporation processes. This conclusion agrees with the one reported in [14] based on the approximate solution of the Boltzmann equation without taking into account the contribution of air in the Knudsen layer.

Acknowledgements

The authors are grateful to A.P. Kryukov, V.Yu. Levashov and M.R. Heikal for their support and useful discussions. EPSRC (Grant EP/C527089/01) (UK) and the Russian Foundation for Basic Research (Grant No. 04-02-16449) (Russia) are acknowledged for the financial support of this project.

References

[1] V.P. Shidlovskiy, Introduction to the Dynamics of Rarefied Gases, American Elsevier Publishing Company, New York, 1967.
[2] H. Grad, On the kinetic theory of rarefied gases, Comm. Pure Appl. Math. 2 (1949) 331.
[3] M.N. Kogan, Rarefied Gas Dynamics, Plenum, New York, 1969.
[4] R.I. Nigmatilin, Dynamics of Multiphase Media, Vol. 1, Hemisphere Publishing Corporation, 1991.
[5] A.I. Akhiezer, I.A. Akhiezer, P.V. Polovin, A.G. Sitenko, K.N. Stepanov, Plasma Electrodynamics, Nauka Publishing House, Moscow, 1974 (in Russian).
[6] S.S. Sazhin, Whistler-mode Waves in a Hot Plasma, Cambridge University Press, 1993.
[7] S.S. Sazhin, Advanced models for fuel droplets heating and evaporation, Progress in Energy and Combustion Science 32 (2006) 162–214.
[8] P.L. Bhatnagar, E.P. Gross, M. Krook, A model for collision processes in gases 1. Small amplitude processes in charged and neutral one component systems, Phys. Rev. 94 (1954) 511–525.
[9] S.S. Sazhin, Cyclotron whistler-mode instability in a collisional plasma, Geomagnetic Research 23 (1978) 105–107 (in Russian).
[10] V.I. Igoshin, V.I. Kurochkin, Laser vaporisation of a metal in a gaseous atmosphere, Quantum Electron. 11 (1984) 1555–1561 (in Russian) (English translation: Sov. J. Quant. Electron. 14 (1984) 1049–1052).
[11] E.M. Shakhov, Methods of Investigation of Rarefied Gas Dynamics, Nauka Publishing House, Moscow (in Russian), 1974.
[12] E.M. Lifshitz, L.P. Pitaevski, Physical Kinetics, Nauka Publishing House, Moscow (in Russian), 1979.
[13] J. Rose, Interphase matter transfer, the condensation coefficient and dropwise condensation, in: Proceedings of 11th International Heat Transfer Conference (August 23–28, 1998, Kyongji, Korea), Vol. 1, Kyongji, Korea, August 23–28, pp. 89–104.
[14] A.P. Kryukov, V.Yu. Levashov, S.S. Sazhin, Evaporation of diesel fuel droplets: kinetic versus hydrodynamic models, Int. J. Heat Mass Transfer 47 (2004) 2541–2549.
[15] G.A. Bird, Molecular Gas Dynamics, Oxford University Press, Oxford, 1976.
[16] G.A. Bird, Molecular Gas Dynamics and the Direct Simulation of Gas Flows, Oxford University Press, Oxford, 1994.
[17] V.V. Aristov, F.G. Tcheremissine, Direct numerical solution of the Boltzmann equation, Computer Centre of Russia Academy of Sciences, Moscow, 1992.
[18] V.V. Aristov, A.P. Kryukov, F.G. Tcheremissine, I.N. Shishkova, Solution of the Boltzmann equation for a plane jet with condensation on a cryogenic panel, J. Comput. Math. Math. Phys. 30 (1991) 1093–1099 (in Russian).
[19] V.V. Aristov, I.N. Shishkova, F.G. Tcheremissine, Solution of the Boltzmann equations for study of inclined shock wave reflection. in: B.D. Shizgal, D.R. Weaver (Eds.), Rarefied Gas Dynamics: Experimental Techniques and Physical Systems, in: Progress in Astronautics and Aeronautics, vol. 158, 1994, pp. 448–461.
[20] F.G. Tcheremissine, Conservative evaluation of Boltzmann collision integral in discrete ordinates approximation, Comput. Math. Appl. 35 (1998) 215–221.
[21] F.G. Tcheremissine, Discrete approximation and examples of the solution of the Boltzmann equation, in: Computational Dynamics of Rarefied Gases, Computer Centre of Russian Academy of Sciences, Moscow 2000, pp. 37–74.
[22] V.V. Aristov, S.P. Popov, F.G. Tcheremissine, I.N. Shishkova, Numerical solution of the Boltzmann and Navier–Stokes equations for a plane jet around a cooled surface, J. Comput. Math. Math. Phys. 36 (1997) 239–242 (in Russian) (English translation: Comp. Math. Math. Phys. 36 (1997) 236–239).
[23] K. Aoki, S. Takata, S. Kosuge, Vapor flows caused by evaporation and condensation on two parallel plane surfaces: effect of the presence of a noncondensable gas, Phys. Fluids 10 (1998) 1519–1533.
[24] S. Kosuge, K. Aoki, S. Takata, Shock-wave structure for a binary gas mixture: finite-difference analysis of the Boltzmann equation for hard-sphere molecules, Eur. J. Mech. B 20 (2001) 87–126.
[25] S. Taguchi, K. Aoki, S. Takata, Vapor flows condensing at incidence onto a plane condensed phase in the presence of noncondensable gas. I. Subsonic condensation, Phys. Fluids 15 (2003) 689–705.
[26] S. Taguchi, K. Aoki, S. Takata, Vapor flows condensing at incidence onto a plane condensed phase in the presence of noncondensable gas. I. Supersonic condensation, Phys. Fluids 16 (2004) 79–92.
[27] A. Raines, Study of a shock wave structure in a gas mixture on the basis of the Boltzmann equation, Eur. J. Mech. B 21 (2002) 599–610.

[28] A.P. Kryukov, V.Yu. Levashov, I.N. Shishkova, Condensation in the presence of a non-condensable component, J. Eng. Phys. Thermophys. 78 (2005) 15–21 (in Russian; English translation is available).
[29] A.P. Kryukov, A.K. Yastrebov, Analysis of transport processes in a vapour film during the interaction between a heated body with cold liquid, Therm. Phys. High Temp. 41 (2003) 771–778 (in Russian).
[30] A.P. Kryukov, V.Yu. Levashov, I.N. Shishkova, A.K. Yastrebov, The Numerical Solution of the Boltzmann Equation for Engineering Applications, Moscow Power Engineering Institute Publishing House, Moscow, 2005.
[31] L.D. Landau, E.M. Lifshitz, Theoretical Physics, Mechanics, vol. 1, Nauka Publishing House, Moscow, 1965 (in Russian).
[32] N.S. Bakhvalov, N.P. Zhidkov, G.M. Kobelkov, Numerical Methods, Nauka Publishing House, Moscow, 1989 (in Russian).
[33] N.M. Korobov, Trigonometric Sums and Their Applications, Nauka Publishing House, Moscow, 1989 (in Russian).
[34] S.P. Popov, F.G. Tcheremissine, Conservative method of the solution of the Boltzmann equation for centrally symmetrical interaction potentials, Computational Mathematics and Mathematical Physics 39 (1999) 163–176.
[35] T. Imamuro, B. Sturtevant, Numerical study of discrete-velocity gases, Phys. Fluids 2 (1990) 2196–2203.
[36] F. Rogier, J.A. Schneider, A direct method for solving the Boltzmann equation, Transport Theory and Statistical Physics 23 (1994) 1–3.
[37] C. Buet, S. Cordier, P. Degond, Regularized Boltzmann operators, Comput. Math. Appl. 35 (1998) 55–74.
[38] F.O. Goodman, H.Y. Wachman, Dynamics of Gas-Surface Scattering, Academic Press, New York, 1976.
[39] S.S. Sazhin, V.V. Serikov, Rarefied gas flows: hydrodynamic versus Monte Carlo modelling, Planetary and Space Science 45 (1997) 361–368.